



Intervalley polaronic biexcitons in metal halide perovskite quantum dots

Ajay K. Poonia,¹ Megha Shrivastava,¹ Wasim J. Mir,² J. Aneesh,¹ Angshuman Nag ,² and K. V. Adarsh ^{1,*}

¹*Department of Physics, Indian Institute of Science Education and Research, Bhopal 462066, India*

²*Department of Chemistry, Indian Institute of Science Education and Research, Pune 411008, India*



(Received 4 August 2020; revised 1 October 2021; accepted 4 October 2021; published 20 October 2021)

The strong band edge exciton-phonon interactions in metal halide perovskite quantum dots (QDs) offer a unique platform to explore many-body phenomena. Employing CsPbBr₃ QDs as a perovskite model system, we report the observation of spin-selective polaronic biexcitons using collective excitations of two circularly polarized ultrafast lasers of a duration that is two orders of magnitude shorter than the exciton lifetime and one order of magnitude shorter than the spin relaxation time. The intervalley polaron pairing of charge carriers determines the anomalously strong exciton-exciton interactions, where the Haynes factor is an order of magnitude larger than the bulk and five times larger than the two-dimensional and quantum well semiconductors, demonstrating a very robust correlation of excitons. Our findings reveal a mechanism of generating highly stable biexciton states even at room temperature to realize higher-order correlations of charge carriers such as quantum droplets and Bose-Einstein condensates.

DOI: [10.1103/PhysRevB.104.L161407](https://doi.org/10.1103/PhysRevB.104.L161407)

Metal halide perovskite (MHP) quantum dots (QDs) crystallized in the APbX₃ lattice [$A = \text{Cs}/\text{Methylammonium} (\text{CH}_3\text{NH}_3^+)/\text{Formamidinium} (\text{CH}(\text{NH}_2)_2^+$) and $X = \text{Cl}/\text{Br}/\text{I}$] have opened a new and unique window to explore static and dynamical quantum phenomena due to their complex electronic structure and strong many-body interactions [1–4]. For instance, a detailed experimental and theoretical analysis revealed an exciton fine structure in which highly emissive and fast decaying bright triplet states lie below the dark singlet state [5]. Another intriguing property of these QDs is the high photoluminescence (PL) quantum yield of near unity due to their distinct defect tolerant electronic structure and reduced surface states [2]. Furthermore, these materials often possess exotic spin properties, such as the Rashba effect [5–12] and spin valleys of contrasting circular dichroism [7], a circular photogalvanic effect [11], and a polarization sensitive optical Stark effect [13]. These exceptional features have led to the emergence of MHP QDs as an outstanding material for various optoelectronic and spintronics applications, such as low-threshold lasing, light-emitting diodes, single-photon emitters, high-efficiency solar cells, and spin devices [1–4,13].

Similar to their bulk counterpart in MHP QDs, the strong coupling of charge carriers to the collective modes of the background phonons in an intrinsically soft polar lattice of MHPs results in large polarons [14–17]. These quasiparticles are dressed charge carriers by phonons and polarized lattice deformation over a few unit cells. The polaronic nature of charge carriers minimizes the scattering between them and defects, resulting in a long carrier lifetime and diffusion length, tolerance to defects, and slow hot carrier relaxation [14–21]. It is theoretically predicted that the exciton-phonon coupling and polarons play a critical role in the formation of correlated

states of carriers such as exciton polarons, exciton condensation, etc., by lowering their ground state energy [22–26]. However, these effects have yet to be explored in MHP QDs and provide a unique opportunity to investigate the many-body physics of photoexcited carriers. In this direction the optical creation of robust multiexciton states such as biexcitons (bound exciton pairs) constitutes a new frontier for this field since their binding energy can be modulated by phonon interactions [22–24]. The eigenstate of the interacting biexciton and phonons can be defined as a polaronic biexciton (PBE). So far, PBE has yet to be observed experimentally, although it constitutes an outstanding problem of many-body systems. Here, we experimentally demonstrate spin-selective PBE, a strongly bound state of biexcitons and phonons in CsPbBr₃ QDs, using the collective excitation of two circularly polarized ultrafast lasers in our transient absorption (TA) spectrometer. The red-detuned pump pulse generates an exciton in a particular spin state, and the probe pulse coherently couples it into a singlet PBE. Our study remarkably reveals an anomalously large Haynes factor (HF) ≈ 1 , which is defined as the ratio of the biexciton to exciton binding energy. We infer that the large biexciton binding energy stems from the intervalley polaron pairing of excitons mediated by a phonon exchange. Apart from the conventional electron-hole attraction, polaron pairing derives the additional correlation of electrons (holes) and leads to an enhanced biexciton binding energy. Further, the exciton spin relaxation follows the Rashba field-induced D'yakonov-Perel' (DP) mechanism, characterizing the intervalley nature of PBE.

CsPbBr₃ QDs used in the present study have a cubic morphology with an average size of 11 nm and lie in the region of a weakly confined system [27]. Details of the sample preparation and characterization can be found in the Supplemental Material (SM) [28]. Figure 1(a) shows the room-temperature optical absorption (OA) of CsPbBr₃ QDs on a microscopic slide. The exciton and continuum contributions are separated

*Corresponding author: adarsh@iiserb.ac.in

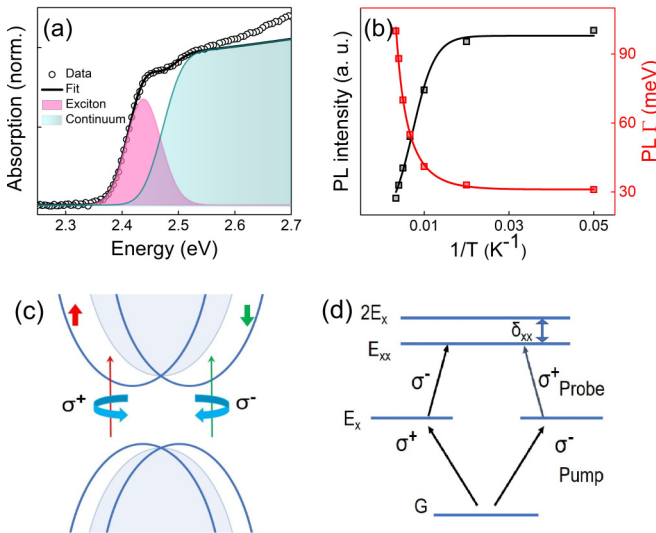


FIG. 1. (a) OA spectrum of CsPbBr₃ QDs at room temperature, fitted with the Elliott model to separate the exciton and continuum contribution. (b) The integrated intensity of the PL peak (black) and PL Γ (red) as a function of temperature, fitted with Eqs. (1) and (2), respectively. (c) Schematic representation for the Rashba splitting of band edges, due to different orbital contributions; the band edges have different magnitudes of splitting at the CB and VB (see text), where \uparrow and \downarrow in the CB correspond to $|+\frac{1}{2}\rangle$ and $|-\frac{1}{2}\rangle$ spin state Rashba valleys. (d) A presentation of biexciton formation with circularly polarized light, where G , E_x , E_{xx} , and δ_{xx} indicate the ground, exciton, biexciton states, and biexciton binding energy, respectively.

by using the Elliott equation for the Wannier-Mott exciton [29] (see details in SM [28]). From the figure, we can see that the exciton peak is centered at 2.435 ± 0.002 eV, with the binding energy (δ_x) 37 ± 2 meV consistent with a previous study [30].

δ_x is further verified from the high-resolution temperature-dependent (20–300 K) PL measurements. Figure 1(b) shows the integrated PL intensity as a function of temperature, which is analyzed with the Arrhenius equation [31,32] to obtain δ_x ,

$$I(T) = \frac{I_0}{1 + Ae^{-\frac{\delta_x}{k_B T}}}, \quad (1)$$

where I_0 and k_B are the PL intensity at 0 K and the Boltzmann constant, respectively. This renders $\delta_x = 32 \pm 3$ meV, consistent with the reported PL and terahertz (THz) measurements [31–33]. Further, the Fröhlich coupling corresponding to the polaron formation is determined from the PL full width at half maximum (Γ) shown in Fig. 1(b) using the equation [31,32]

$$\Gamma(T) = \Gamma_0 + \frac{\gamma_{LO}}{e^{\frac{E_{LO}}{k_B T}}} - 1, \quad (2)$$

where Γ_0 , E_{LO} , and γ_{LO} are temperature-independent line broadening, longitudinal optical (LO) phonon energy, and the exciton-phonon interaction strength, respectively. The best fit to the experimental data shows γ_{LO} and E_{LO} are 64 ± 12 and 17 ± 2 meV. The obtained parameter γ_{LO} is in accordance with the intermediate to large exciton-phonon

coupling regime that is consistent with the previous report [12]. Recently, it is shown that the LO phonon (18 meV) is responsible for the large polaron in the bulk and QDs of CsPbBr₃ [14,16].

After discussing the exciton binding energy and their phonon coupling, we experimentally generate the biexciton states by exploiting the unique band structure and spin selection rules. For instance, in CsPbBr₃, the top of the valence band (VB) consists of Pb 6s and Br 4p atomic orbitals with an overall s symmetry, and the conduction band (CB) primarily comprises of Pb 6p orbitals. The strong spin-orbit coupling (SOC) makes the band edge states doubly degenerate where electrons can occupy $|\pm\frac{1}{2}\rangle$ spin states. This, combined with the lack of structural symmetry, leads to the Rashba effect, forming shallow spin valleys at the Γ symmetry point [5–12]. The schematics of the spin valleys and the associated optical selection rules are shown in Fig. 1(c); here, the \uparrow and \downarrow arrows represent the $|+\frac{1}{2}\rangle$ and $|-\frac{1}{2}\rangle$ spin Rashba valleys. The presence of spin states in CsPbBr₃ QDs offers an ideal platform for the coherent spin-selective generation of the biexciton with zero net spin [34,35]. The governing spin selection rules are $\Delta J = 0$ and $\Delta m_j = \pm 1$, as shown in Figs. 1(c) and 1(d). This provides an extremely efficient method for generating a spin-selective biexciton in which two excitons of opposite spin pair to form a biexciton that can be accessed optically. For instance, the absorption of the right circularly polarized (σ^+) pump pulse will produce excitons in the $|+\frac{1}{2}\rangle$ spin state. Then, the second sequential probe pulse of opposite helicity (σ^-) of the pump pulse promotes the remaining $|+\frac{1}{2}\rangle$ VB electrons to the $|-\frac{1}{2}\rangle$ CB and converts the exciton population into a biexciton. The spin selection rules prohibit the biexciton formation for cocircular polarization [34,35]. Based on the above discussion, first, we have generated a spin-polarized exciton by using a 100-fs σ^+ pump pulse centered at 2.38 eV with a fluence of $2 \mu\text{J}/\text{cm}^2$. The exciton is coherently converted into a biexciton by using the σ^- probe pulse (1.55–2.75 eV). The duration of the pump-probe pulses is much shorter than the relaxation time of the exciton (few ns) [36] and spin (few ps, discussed later). Hence, the coupled exciton pair can be safely viewed as an isolated two-level system. Figure 2(a) displays the contour plot of TA at room temperature when the two pulses are cross-circular polarized ($\sigma^+\sigma^-$).

The complex TA can be better described as bleach (≈ 2.42 eV) at the exciton position, induced absorptions (IA_1) (blue side), and IA_2 (red side) of the exciton bleach. Figure 2(b) shows the TA spectrum of the ($\sigma^+\sigma^+$), which is used to distinguish the biexciton signal. On the basis of it, we identify IA_2 as arising from the biexciton. The bleach assigned to the phase space filling of the exciton and IA_1 to the exciton-polaron induced transition [28,37] are present in both polarization and even for neutral polarization (Fig. S3), indicating their common origin (see details in SM [28]). The occurrence of a biexciton in the case of the opposite spin pairing of the excitons lowers the energy of the bound state and redshifts the transition, which is consistent with the attractive interaction between the excitons.

After demonstrating the generation of a biexciton, however, their usefulness would be rather limited without knowing the binding energy (δ_{xx}). For this, we plotted the ΔA for

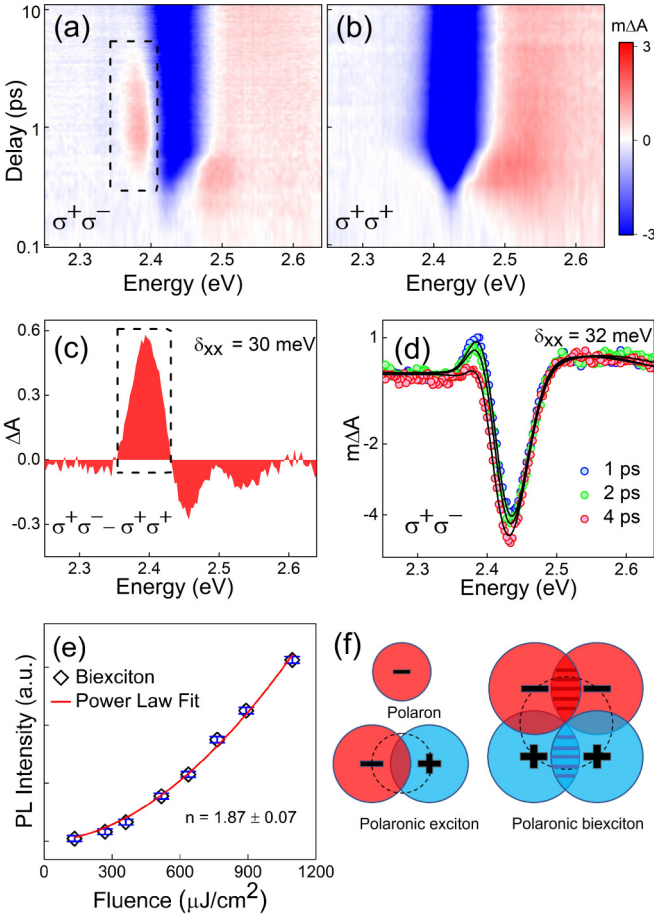


FIG. 2. The contour plot of TA at 300 K for (a) $\sigma^+\sigma^-$ and (b) $\sigma^+\sigma^+$, where in $\sigma^+\sigma^-$ a strong redshifted IA appears corresponding to the spin-selective biexciton, in the dashed rectangular box. (c) Difference of ($\sigma^+\sigma^- - \sigma^+\sigma^+$), where the biexciton absorption is centered at 2.39 eV, enclosed in a rectangular box. (d) The spectral evolution of TA at various time delays, where the solid black lines show the fit using Eq. (3). (e) Power-law fitting of peak biexciton (BX) intensity revealing a near-quadratic intensity dependence with exponent $n = 1.87 \pm 0.07$, indicating that it is due to biexciton emission. (f) A simplified picture of PBE, where the red and blue circles show the polaron cloud associated with the electron ($-$) and hole ($+$), respectively. The polaron coupling is indicated by the solid horizontal lines at the overlapping area of two large polarons associated with different excitons.

($\sigma^+\sigma^- - \sigma^+\sigma^+$) in Fig. 2(c). The absorption feature corresponding to the biexcitons is centered at 2.39 eV, with $\delta_{xx} \approx 30$ meV. To further verify this value and for a more precise determination, we fitted the TA using the following equation [36],

$$TA = y_0 + NAe^{-\left(\frac{x-x_0-\delta_{xx}}{w_e}\right)^2} - Ae^{-\left(\frac{x-x_0}{w_g}\right)^2}, \quad (3)$$

where A , x_0 , N , w , and subscripts e and g are the amplitude of the exciton transition, peak position, oscillator strength, width of the Gaussian, and excited and ground states, respectively. The best fit to the experimental data shown in Fig. 2(d) reveals $\delta_{xx} = 32 \pm 2$ meV. This value is similar to our previous results obtained with 400 nm excitation [36]. To further analyze the biexciton, we have investigated the PL intensity at different

TABLE I. Value of HF for different classes of semiconductors.

Sample	HF
CsPbBr ₃ QDs	≈ 1
Monolayer WSe ₂	0.14 [41]
GaAs quantum well	0.20 [42]
Bulk semiconductor	0.10 [38]

excitation fluences under a pump excitation of 3.1 eV. The obtained spectra are shown in Fig. S9. It shows that at low fluence PL exhibits a single-component emission from the exciton state while for high pump fluence we observe two-component emission. To verify the nature of this low-energy emission we have plotted the peak amplitude at various excitation fluences [Fig. 2(e)]. It reveals a nearly quadratic intensity dependence with $n = 1.87 \pm 0.07$, which confirms it is associated with the biexciton. The binding energy obtained by this method is 40 ± 3 meV (see details in SM [28]).

Remarkably, the biexciton binding energy is anomalously large and nearly equal to the exciton binding energy at room temperature. To show the usefulness of this hallmark result and to make a quantitative comparison with other materials, we determined the Haynes factor (HF), defined as the ratio of biexciton to exciton binding energy (δ_{xx}/δ_x) [38]. CsPbBr₃ QDs show a large HF = 0.9 ± 0.1 , consistent with our recent study [39] in strongly confined CsPbBr₃ QDs and a previous reported value in CsPbBr₃ nanoplatelets [40]. It is an order of magnitude larger than in the bulk semiconductors and five times larger than in the two-dimensional (2D) and quantum well semiconductors. For a comparison, HF values of different materials are listed in Table I. This result seems to be compelling since the biexciton binding energy is anomalously large in the weakly confined CsPbBr₃ QDs, and can be used for biexciton lasing and polarization entanglement. Explaining and understanding the origin of the biexciton and its huge HF is of major importance for many potential applications. For this, first, we considered the tomography of the biexciton, which is a bound system of two electrons and two holes (bound exciton pair), and the composite quasiparticle is stable under the effect of Coulomb interactions [electron-hole attraction and electron-electron (hole-hole) repulsion]. This highlights the importance of having a robust exciton to observe a biexciton. A typical example is 2D transition metal dichalcogenides, where strongly confined excitons having a binding energy of 300–500 meV lead to a biexciton binding energy of 40–60 meV [41,43]. However, what we observed in CsPbBr₃ QDs is nearly the same binding energy of the exciton and biexciton that cannot be explained based only on the many-body theory of exciton interactions. To explain our result, we propose a framework of a biexciton by incorporating the polaron effect, which is generally not considered in conventional QDs due to its comparatively weak effect. But in the case of MHP QDs, polarons and excitons have the same range of parameters (binding energy and radius), which is discussed below. The presence of polarons with a considerably large binding energy [16] suggests another type of coupling of charge carriers mediated by the phonon exchange and leads to the pairing of the same charge carriers. These coupled same

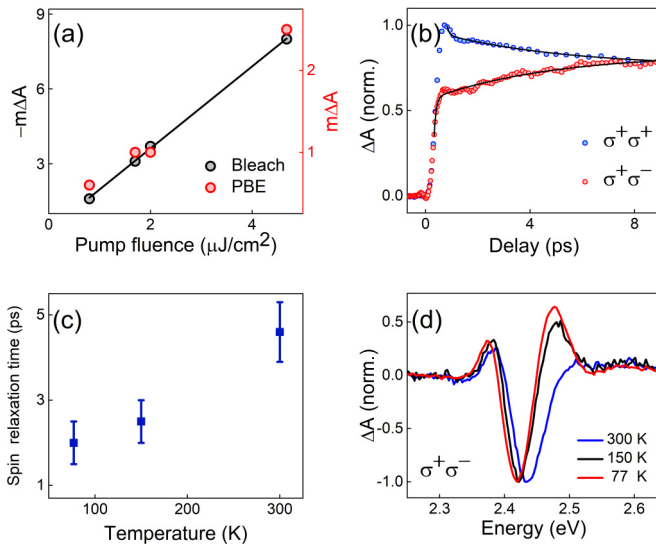


FIG. 3. (a) Amplitude of exciton bleach and PBE with pump fluence showing the linear region of the experiment. (b) Kinetics of spin relaxation at the position of bleach for room temperature. (c) Spin relaxation time at different temperatures indicating that time for spin relaxation decreases at low temperatures due to the DP mechanism. (d) Spectral evolution of TA (at 1 ps) at various temperatures for $\sigma^+\sigma^-$, showing the strong emergence of blueshifted absorption at low temperatures.

charge carriers (electron-electron and hole-hole) are generally known as bipolarons [44] and have been previously observed for the other members of the perovskite family [45–47] but not considered in the framework of biexcitons. By incorporating both the exciton and polaron effects, we suggest that a biexciton system can be further stable under the strong correlation of electrons (holes). It means that due to the presence of a polarization field there will be an attractive interaction between the electron-electron and hole-hole [44], which acts to stabilize the biexciton. A schematic of the polaronic coupling of excitons and biexcitons is shown in Fig. 2(f).

Further, we determine the polaron parameters [16], namely the Fröhlich constant (α), polaron binding energy (E_P), and radius (R_P) within Feynman’s model, given by $\alpha = \frac{e^2}{4\pi\epsilon\hbar} \left(\frac{1}{\epsilon_\infty} - \frac{1}{\epsilon_0} \right) \sqrt{\frac{m^*}{2E_{LO}}}$, $E_P = E_{LO}(\alpha + 0.0123\alpha^2)$, and $R_P = \left(\frac{3.4\hbar}{m^*\alpha\omega_{LO}} \right)^{\frac{1}{2}}$. Here, ϵ , ϵ_∞ , ϵ_0 , m^* , and ω_{LO} are the dielectric constant of vacuum, the optical dielectric constant, the static dielectric constant of the medium, the effective mass of the carrier, and the angular frequency of the LO phonon. Using the value of the dielectric constant from THz spectroscopy [33] and the effective mass from a first-principles calculation [16,33] for a LO phonon of 17 meV we have estimated $\alpha = 1.2$ –1.3, $E_P = 20$ –23 meV, and $R_P = 7.2$ –8.8 nm. The relatively same range of exciton and polaron parameters clearly indicates that the polarization clouds linked with electrons and holes are comparable to the spatial distribution of the composite biexciton system, hence leading to the polaronic coupling of two excitons at room temperature in the linear regime of excitation [Fig. 3(a)].

Furthermore, we examine the spin dynamics of carriers which plays a key role in the spin-selective biexciton forma-

tion. For this purpose, we carried out our measurements from room to low temperatures. The spin relaxation of carriers, in both the spin states ($|\pm\frac{1}{2}\rangle$), can be deterministically monitored by σ^+ and σ^- probes. For instance, the σ^+ pump populates excitons in the $|+\frac{1}{2}\rangle$ state, and then the probe of σ^+ or σ^- selectively detects the bleach of $|+\frac{1}{2}\rangle$ and $|-\frac{1}{2}\rangle$ states. From this, we can estimate the spin relaxation time from the decay of bleach in the $|+\frac{1}{2}\rangle$ state and the growth of bleach in the $|-\frac{1}{2}\rangle$ state. Figure 3(b) presents the decay of exciton bleach in $|+\frac{1}{2}\rangle$ and the simultaneous growth of bleach in the $|-\frac{1}{2}\rangle$ states due to a spin flip. This simultaneous decay and rise of the $|+\frac{1}{2}\rangle$ and $|-\frac{1}{2}\rangle$ states reach equilibrium within 8 ps. Spin relaxation time, defined as the average time of bleach decay and growth, is plotted against temperatures in Fig. 3(c). From the figure, it can be noticed that the spin relaxation time increases with an increase in the temperature. The observed temperature dependence behavior is consistent with the previous measurement of spin relaxation in CsPbBr₃ thin films [9] and follows the DP spin relaxation mechanism, which applies to systems that have SOC and a lack of inversion symmetry [48]. In the absence of symmetry, the SOC induces an effective magnetic field (Rashba effect), which drives the precessional spin relaxation of the excitons. At low temperatures, due to a reduced scattering of excitons and a more prominent Rashba effect, spin relaxation takes place rapidly. It is not related to any phase transition as verified from the temperature-dependent x-ray diffraction (XRD) (Fig. S1), where no phase transition is observed in the range of our measurements [49].

Lattice symmetry breaking which derives the Rashba field is also observed to affect the IA₁ transition of excitons which was weak at 300 K. Figure 3(d) shows the spectral evolution of $\sigma^+\sigma^-$ as a function of temperature. From the figure, it can be noticed that TA features are the same, but IA₁ is more prominent at low temperatures. These transitions are parity controlled and take place in the presence of symmetry breaking but forbidden in the equilibrium conditions [37,50] (see details in SM [28]). These results are similar to those observed in the small size QDs where polaron-induced lattice distortion activates the forbidden transition [37]. Strikingly, the same feature is observed in our system at low temperatures, indicating that polaron-induced symmetry breaking is more prominent at low temperatures [28,51–53].

In summary, we have demonstrated the robust intervalley PBE at room temperature in CsPbBr₃ QDs. In our experiments, a red-detuned circularly polarized pump pulse generates an exciton in a particular spin state, and the probe pulse coherently converts it into spin-selective PBE with an anomalously large HF ≈ 1 , indicating the exciton and biexciton binding energy are nearly the same. We infer that the strong exciton-exciton interaction stems from the intervalley polaron pairing of excitons, which derives the attractive interaction between electrons (holes). Our finding suggests a key role of biexcitons in MHP QDs and shows the possibility of many exotic phenomena, such as the biexciton mediated optical Stark effect and stimulated emission from the biexciton state. Further, a strong lattice effect will help to realize the higher-order correlations of charge carriers such as quantum droplets, and Bose-Einstein condensates of the biexciton at room temperature.

The authors gratefully acknowledge the Science and Engineering Research Board (Project No. CRG/2019/002808), DAE BRNS (Sanction No. 37(3)/14/26/2016-BRNS/37245), and FIST Project for Department of Physics.

The authors also gratefully acknowledge the support of Dr. Matthew C. Beard and Dr. Haipeng Lu of NREL. K.V.A. gratefully acknowledges support from a DST-IUSSTF BASE fellowship.

- [1] J. Huang, Y. Yuan, Y. Shao, and Y. Yan, *Nat. Rev. Mater.* **2**, 17042 (2017).
- [2] Q. A. Akkerman, G. Rainó, M. V. Kovalenko, and L. Manna, *Nat. Mater.* **17**, 394 (2018).
- [3] Y. Fu, H. Zhu, J. Chen, M. P. Hautzinger, X.-Y. Zhu, and S. Jin, *Nat. Rev. Mater.* **4**, 169 (2019).
- [4] H. Utzat, W. Sun, A. E. K. Kaplan, F. Krieg, M. Ginterseder, B. Spokoiny, N. D. Klein, K. E. Shulenberg, C. F. Perkinson, M. V. Kovalenko, and M. G. Bawendi, *Science* **363**, 1068 (2019).
- [5] M. A. Becker, R. Vaxenburg, G. Nedelcu, P. C. Sercel, A. Shabaev, M. J. Mehl, J. G. Michopoulos, S. G. Lambrakos, N. Bernstein, J. L. Lyons, T. Stöferle, R. F. Mahrt, M. V. Kovalenko, D. J. Norris, G. Rainó, and A. L. Efros, *Nature (London)* **553**, 189 (2018).
- [6] M. Isarov, L. Z. Tan, M. I. Bodnarchuk, M. V. Kovalenko, A. M. Rappe, and E. Lifshitz, *Nano Lett.* **17**, 5020 (2017).
- [7] B. Wu, H. Yuan, Q. Xu, J. A. Steele, D. Giovanni, P. Puech, J. Fu, Y. F. Ng, N. F. Jamaludin, A. Solanki, S. Mhaisalkar, N. Mathews, M. B. J. Roeloffs, M. Grätzel, J. Hofkens, and T. C. Sum, *Nat. Commun.* **10**, 484 (2019).
- [8] H. Ryu, D. Y. Park, K. M. McCall, H. R. Byun, Y. Lee, T. J. Kim, M. S. Jeong, J. Kim, M. G. Kanatzidis, and J. I. Jang, *J. Am. Chem. Soc.* **142**, 21059 (2020).
- [9] M. Zhou, J. S. Sarmiento, C. Fei, X. Zhang, and H. Wang, *J. Phys. Chem. Lett.* **11**, 1502 (2020).
- [10] S. D. Stranks and P. Plochocka, *Nat. Mater.* **17**, 381 (2018).
- [11] P. A. Obraztsov, D. Lyashenko, P. A. Chizhov, K. Konishi, N. Nemoto, M. Kuwata-Gonokami, E. Welch, A. N. Obraztsov, and A. Zakhidov, *Commun. Phys.* **1**, 14 (2018).
- [12] J. A. Steele, P. Puech, B. Monserrat, B. Wu, R. X. Yang, T. Kirchartz, H. Yuan, G. Fleury, D. Giovanni, E. Fron, M. Keshavarz, E. Debroye, G. Zhou, T. C. Sum, A. Walsh, J. Hofkens, and M. B. J. Roeloffs, *ACS Energy Lett.* **4**, 2205 (2019).
- [13] K. Liao, X. Hu, Y. Cheng, Z. Yu, Y. Xue, Y. Chen, and Q. Gong, *Adv. Opt. Mater.* **7**, 1900350 (2019).
- [14] O. Cannelli, N. Colonna, M. Puppini, T. C. Rossi, D. Kinschel, L. M. D. Leroy, J. Löffler, J. M. Budarz, A. M. March, G. Doumy, A. Al Haddad, M.-F. Tu, Y. Kumagai, D. Walko, G. Smolentsev, F. Krieg, S. C. Boehme, M. V. Kovalenko, M. Chergui, and G. F. Mancini, *J. Am. Chem. Soc.* **143**, 9048 (2021).
- [15] E. Cinquanta, D. Meggiolaro, S. G. Motti, M. Gandini, M. J. P. Alcocer, Q. A. Akkerman, C. Vozzi, L. Manna, F. De Angelis, A. Petrozza, and S. Stagira, *Phys. Rev. Lett.* **122**, 166601 (2019).
- [16] M. Puppini, S. Polishchuk, N. Colonna, A. Crepaldi, D. N. Dirin, O. Nazarenko, R. De Gennaro, G. Gatti, S. Roth, T. Barillot, L. Poletto, R. P. Xian, L. Rettig, M. Wolf, R. Ernstorfer, M. V. Kovalenko, N. Marzari, M. Grioni, and M. Chergui, *Phys. Rev. Lett.* **124**, 206402 (2020).
- [17] H. Seiler, S. Palato, C. Sonnichsen, H. Baker, E. Socie, D. P. Strandell, and P. Kambhampati, *Nat. Commun.* **10**, 4962 (2019).
- [18] X.-Y. Zhu and V. Podzorov, *J. Phys. Chem. Lett.* **6**, 4758 (2015).
- [19] K. Miyata, T. L. Atallah, and X. Y. Zhu, *Sci. Adv.* **3**, e1701469 (2017).
- [20] H. Zhang, E. Debroye, J. A. Steele, M. B. J. Roeloffs, J. Hofkens, H. I. Wang, and M. Bonn, *ACS Energy Lett.* **6**, 568 (2021).
- [21] M. Schlipf, S. Poncé, and F. Giustino, *Phys. Rev. Lett.* **121**, 086402 (2018).
- [22] G. Beni and T. M. Rice, *Phys. Rev. Lett.* **37**, 874 (1976).
- [23] L. V. Keldysh and A. P. Silin, *Zh. Eksp. Teor. Fiz.* **69**, 1053 (1975) [*Sov. Phys. JETP* **42**, 535 (1976)].
- [24] A. R. Srimath Kandada and C. Silva, *J. Phys. Chem. Lett.* **11**, 3173 (2020).
- [25] M. Ueta, H. Kanzaki, K. Kobayashi, Y. Toyozawa, and E. Hanamura, *Excitonic Processes in Solids* (Springer, Berlin, 1986).
- [26] O. Verzele, R. Ferreira, and G. Bastard, *Phys. Rev. Lett.* **88**, 146803 (2002).
- [27] L. Protesescu, S. Yakunin, M. I. Bodnarchuk, F. Krieg, R. Caputo, C. H. Hendon, R. X. Yang, A. Walsh, and M. V. Kovalenko, *Nano Lett.* **15**, 3692 (2015).
- [28] See Supplemental Material at <http://link.aps.org/supplemental/10.1103/PhysRevB.104.L161407> for sample preparation and characterization, exciton binding energy, experiment setup, neutral polarized TA and IA₁, expression for the polaron coupling, schematic diagram of the biexciton for small polarons, spectral evolution of cocircular polarization at different temperatures, spin relaxation, polaron stability at low temperature, and excitation-dependent PL.
- [29] R. J. Elliott, *Phys. Rev.* **108**, 1384 (1957).
- [30] B. J. Bohn, Y. Tong, M. Gramlich, M. L. Lai, M. Döblinger, K. Wang, R. L. Z. Hoyer, P. Müller-Buschbaum, S. D. Stranks, A. S. Urban, L. Polavarapu, and J. Feldmann, *Nano Lett.* **18**, 5231 (2018).
- [31] J. Li, X. Yuan, P. Jing, J. Li, M. Wei, J. Hua, J. Zhao, and L. Tian, *RSC Adv.* **6**, 78311 (2016).
- [32] A. Shinde, R. Gahlaut, and S. Mahamuni, *J. Phys. Chem. C* **121**, 14872 (2017).
- [33] G. R. Yettapu, D. Talukdar, S. Sarkar, A. Swarnkar, A. Nag, P. Ghosh, and P. Mandal, *Nano Lett.* **16**, 4838 (2016).
- [34] W. Schäfer and M. Wegener, *Semiconductor Optics and Transport Phenomena* (Springer, Berlin, 2002).
- [35] A. Steinhoff, M. Florian, A. Singh, K. Tran, M. Kolarczik, S. Helmrich, A. W. Achtstein, U. Woggon, N. Owschimikow, F. Jahnke, and X. Li, *Nat. Phys.* **14**, 1199 (2018).
- [36] J. Aneesh, A. Swarnkar, V. Kumar Ravi, R. Sharma, A. Nag, and K. V. Adarsh, *J. Phys. Chem. C* **121**, 4734 (2017).

- [37] D. Rossi, H. Wang, Y. Dong, T. Qiao, X. Qian, and D. H. Son, *ACS Nano* **12**, 12436 (2018).
- [38] J. Singh, D. Birkedal, V. G. Lyssenko, and J. M. Hvam, *Phys. Rev. B* **53**, 15909 (1996).
- [39] M. Shrivastava, F. Krieg, D. Mandal, A. K. Poonia, S. K. Bera, M. V. Kovalenko, and K. V. Adarsh (unpublished).
- [40] J. Chen, Q. Zhang, J. Shi, S. Zhang, W. Du, Y. Mi, Q. Shang, P. Liu, X. Sui, X. Wu, R. Wang, B. Peng, H. Zhong, G. Xing, X. Qiu, T. C. Sum, and X. Liu, *Commun. Phys.* **2**, 80 (2019).
- [41] Y. You, X.-X. Zhang, T. C. Berkelbach, M. S. Hybertsen, D. R. Reichman, and T. F. Heinz, *Nat. Phys.* **11**, 477 (2015).
- [42] D. Birkedal, J. Singh, V. G. Lyssenko, J. Erland, and J. M. Hvam, *Phys. Rev. Lett.* **76**, 672 (1996).
- [43] E. J. Sie, A. J. Frenzel, Y.-H. Lee, J. Kong, and N. Gedik, *Phys. Rev. B* **92**, 125417 (2015).
- [44] D. Emin, *Polarons* (Cambridge University Press, Cambridge, UK, 2012).
- [45] V. N. Kostur and P. B. Allen, *Phys. Rev. B* **56**, 3105 (1997).
- [46] J. Shamblin, M. Heres, H. Zhou, J. Sangoro, M. Lang, J. Neufeind, J. A. Alonso, and S. Johnston, *Nat. Commun.* **9**, 86 (2018).
- [47] H. Ouhbi, F. Ambrosio, F. De Angelis, and J. Wiktor, *J. Phys. Chem. Lett.* **12**, 5339 (2021).
- [48] I. Žutić, J. Fabian, and S. Das Sarma, *Rev. Mod. Phys.* **76**, 323 (2004).
- [49] P. Cottingham and R. L. Brutchey, *Chem. Mater.* **30**, 6711 (2018).
- [50] M. C. Brennan, J. E. Herr, T. S. Nguyen-Beck, J. Zinna, S. Draguta, S. Rouvimov, J. Parkhill, and M. Kuno, *J. Am. Chem. Soc.* **139**, 12201 (2017).
- [51] O. Verzelen, R. Ferreira, and G. Bastard, *Phys. Rev. B* **62**, R4809 (2000).
- [52] S. Sauvage, P. Boucaud, R. P. S. M. Lobo, F. Bras, G. Fishman, R. Prazeres, F. Glotin, J. M. Ortega, and J.-M. Gérard, *Phys. Rev. Lett.* **88**, 177402 (2002).
- [53] S. Anand, P. Verma, K. P. Jain, and S. C. Abbi, *Phys. B: Condens. Matter* **226**, 331 (1996).